

Visual Position Prompt for MLLM based Visual Grounding

Wei Tang[†], Yanpeng Sun, Qinying Gu, and Zechao Li, *Senior Member, IEEE*

Abstract—Although Multimodal Large Language Models (MLLMs) excel at various image-related tasks, they encounter challenges in precisely aligning coordinates with spatial information within images, particularly in position-aware tasks such as visual grounding. This limitation arises from two key factors. First, MLLMs lack explicit spatial references, making it difficult to associate textual descriptions with precise image locations. Second, their feature extraction processes prioritize global context over fine-grained spatial details, leading to weak localization capability. To address this issue, we introduce VPP-LLaVA, an MLLM equipped with Visual Position Prompt (VPP) to improve its grounding capability. VPP-LLaVA integrates two complementary mechanisms. The global VPP overlays learnable, axis-like embeddings onto the input image to provide structured spatial cues. The local VPP focuses on fine-grained localization by incorporating position-aware queries, which suggests probable object locations. We also introduce a VPP-SFT dataset with 0.6M samples, consolidating high-quality visual grounding data into a compact format for efficient model training. Training on this dataset with VPP enhances the model’s performance, achieving state-of-the-art results on standard grounding benchmarks despite using fewer training samples compared to other MLLMs like MiniGPT-v2, which rely on much larger datasets (~21M samples). The code and VPP-SFT dataset will be available at <https://github.com/WayneTomas/VPP-LLaVA> upon acceptance.

Index Terms—Multimodal large language model, Visual grounding, Visual prompt, Prompt learning.

I. INTRODUCTION

MULTI-MODAL Large Language Models (MLLMs) [1], [2], [3], [4], [5] achieve impressive results across various image-related tasks [6], [7], [8], [9], earning considerable attention from the research community. Among these tasks, visual grounding—specifically Referring Expression Comprehension (REC)—stands out as a critical challenge [10], [11], [12], [7], [13]. Unlike pure detection tasks [14], [15], [16], visual grounding involves precisely identifying locations within an image based on free-form language expressions. It is fundamental for cognitive interactions between humans and machines, with applications such as image segmentation [17], remote sensing [18] and human-robot interaction [19].

While research [20], [21] indicates that MLLMs possess a reasonable ability for spatial understanding, there is a growing

W. Tang, Y. Sun and Z. Li are with School of Computer Science and Engineering, Nanjing University of Science and Technology, No.200 Xiaolingwei Road, Nanjing 210094, China. E-mail: {weitang, zechao.li and yanpeng_sun}@njust.edu.cn (Corresponding authors: Zechao Li and Qinying Gu)

Q. Gu are with Shanghai Artificial Intelligence Laboratory, No.129 Longwen Road, Shanghai 200232, China. E-mail: guqinying@pjlab.org.cn.

[†] This work was done during his internship at Shanghai Artificial Intelligence Laboratory.

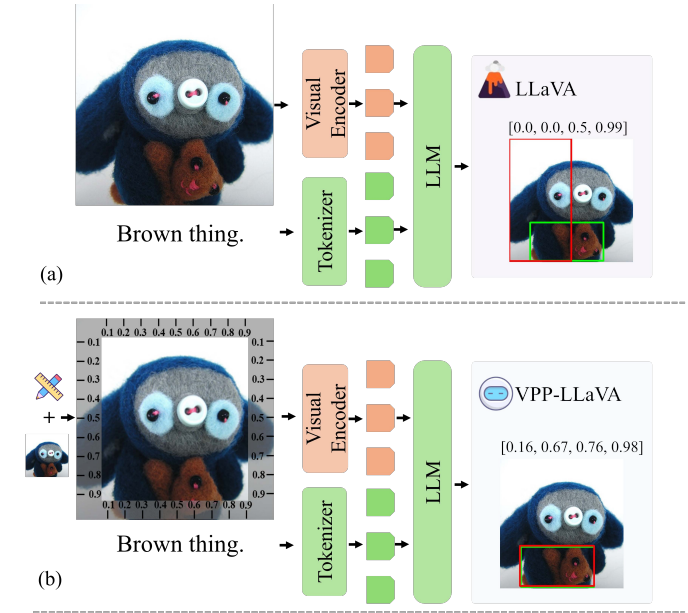


Fig. 1. A visual grounding case study of MLLMs: (a) LLaVA-v1.5 outputs an inaccurate bounding box based on the given query expression. (b) When provided with a position reference, VPP-LLaVA produces a suitable result. For brevity, some text instructions are omitted.

consensus that these models still require further enhancement, particularly for tasks involving precise spatial reasoning like visual grounding. As illustrated in Fig. 1 (a), the grounding results from LLaVA-v1.5, for instance, reveal notable inaccuracies (the red box indicates the predicted bounding box, while the green box represents the ground truth). Although the predicted bounding box partially covers the target object, i.e., the brown toy, it suffers from both size and shape inaccuracies, failing to align well with the object’s true boundaries. These limitations highlight the need for more effective strategies to improve spatial alignment and object localization in MLLMs. To address these challenges, some studies are investigating the integration of advanced region-level enhancement modules and larger, more comprehensive visual grounding datasets into MLLMs [13], [22], [23], [6]. Other approaches are exploring the incorporation of task-specific expertise, such as converting special tokens directly into bounding boxes with additional decoder, to improve localization accuracy [24], [25].

However, despite the use of the aforementioned methods to enhance MLLM performance in grounding tasks, studies suggest that MLLMs still face significant challenges in precisely aligning coordinates with spatial information in images [26], [27]. One key issue lies in the models’ ability to effectively

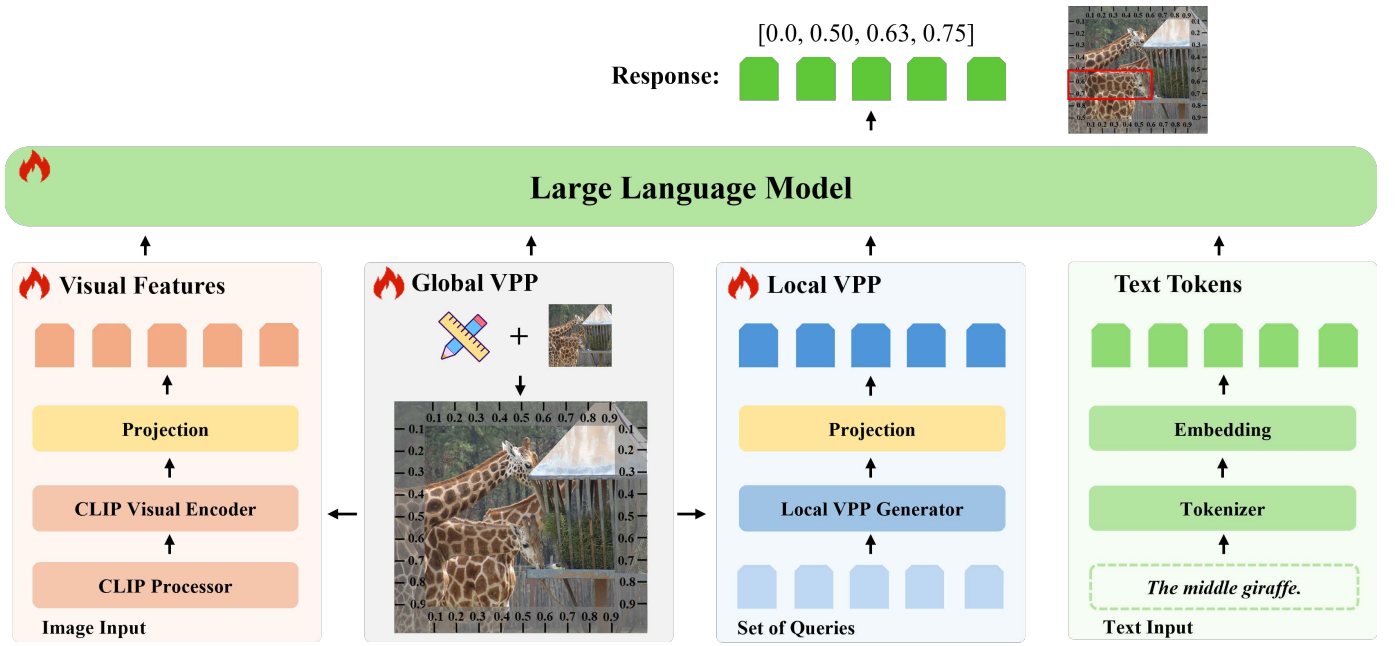


Fig. 2. An illustration of VPP-LLaVA, an MLLM-based visual grounding framework with Visual Position Prompt (VPP). We utilize the global VPP to provide a global position reference for MLLMs with foundational spatial cues. Additionally, a local VPP, serving as a local position reference, is introduced to further enhance and incorporate object spatial information. For brevity, some text instructions are omitted.

interpret and utilize spatial cues, which remain underutilized in many cases. As shown in Fig. 1 (b), when we introduce a positional reference in the form of a coordinate axis, providing an explicit spatial guide, the model’s understanding of spatial relationships improves significantly. This reference allows the model to better interpret the spatial information of objects in the image, leading to more accurate localization. Specifically, the predicted bounding box becomes more aligned with the brown toy, reflecting the improved spatial reasoning and localization accuracy when positional references are incorporated.

Based on these observations, we propose integrating positional references as prompts within MLLMs to improve their visual grounding capabilities. While the coordinate axis shown in Fig. 1 (b) provides a global spatial guide, we also explore the potential of leveraging object position embeddings, derived from detection models, which offer local spatial cues by capturing object locations and semantic context. These two types of Visual Position Prompt (VPP)—global and local—are complementary, with the global guide helping to establish overall spatial structure, and the local cues refining object-specific localization.

Specifically, the global VPP is initialized in an axis-like form and overlaid onto the input image, providing a global spatial reference. This enables MLLMs to more effectively align coordinate information with spatial details across the image. To capture object-specific spatial and semantic information, we introduce a local VPP, which identifies potential objects within the image. This local reference helps the decoder integrate object-level details with other features. By combining both global and local prompts, our model improves spatial alignment and boosts performance in visual grounding tasks. Notably, we achieve state-of-the-art results with a relatively

small training set of about 0.6M samples from our new VPP-SFT dataset, which consolidates high-quality visual grounding data into a compact form. Compared to other MLLMs like MiniGPT-v2, which require around ~ 21 M grounding samples, our approach demonstrates superior efficiency while maintaining strong performance.

In summary, our contributions are shown as follows:

- We propose VPP-LLaVA, an MLLM-based method for visual grounding with a Visual Position Prompt, along with a high-quality grounding instruction tuning dataset, VPP-SFT, which contains approximately 0.6M samples.
- We introduce novel global and local Visual Position Prompts that enable MLLMs to more effectively link spatial information within images to coordinate details, thereby enhancing their visual grounding capabilities.
- Extensive experiments demonstrate that our method not only achieves state-of-the-art performance but also does so with a substantially smaller training dataset compared to other MLLMs, highlighting its efficiency.

II. RELATED WORK

A. Visual Grounding

Visual grounding is a fundamental vision-language task that locates objects in an image based on a given free-formed linguistic expression [28].

Conventional methods. Conventional visual grounding methods are typically divided into three categories [29]: two-stage methods [30], [31], [32], one-stage methods [33], [34], and transformer-based methods [35], [29], [36], [12], [37], [38]. In pioneering two-stage methods such as EARN [30] and MattNet [31], a standard detection network generates region proposals, and the proposal that best matches the language

query is selected through cross-modal matching. Due to the limitations of pre-trained detectors, one-stage methods are increasingly being adopted as an alternative solution. For example, FAOA, which is based on YOLOv3, is presented in [33]. it generates the bounding box using a YOLO-like network based on the fused features from visual and linguistic modalities. With the advancement of Vision-Language Pre-trained (VLP) models, transformer-based methods are becoming increasingly popular for their strong performance and independence from pre-defined anchors, which is typical of one-stage methods. TransVG [39], VLTVG [35], TransCP [29], MDETR [36], CLIP-VG [12], OFA [37], and UNINEXT-L [38] are among the most representative methods. These methods directly fuse visual and linguistic features using a transformer and model visual grounding as a regression task. Despite the significant progress made by conventional methods in the field of visual grounding, these approaches are often specifically designed for individual tasks. Recently, researchers have shifted their focus toward Multimodal Large Language Models (MLLMs), leveraging their ability to unify visual grounding with other vision-related tasks. This integration streamlines task handling within a single, versatile model.

MLLM-based methods. With the tremendous success of LLMs in the field of natural language processing [40], [41], researchers are considering expanding their application to the multimodal domain [2], [3]. LLaVA [2] and MiniGPT-4 [42] are typical examples of such efforts. However, they still have room for improvement in the field of visual grounding. To enhance MLLMs' grounding capability, researchers are proposing the incorporation of more visual grounding data and advanced position-aware modules. For example, Shikra [20], Kosmos [43], and MiniGPT-v2 [13] discrete coordinates into specialized tokens to better align with MLLMs' input formats. Ferret [7] introduces a Spatial-Aware Visual Sampler, while PINK [44] employs a self-consistent bootstrapping approach to enhance region sensitivity. These methods still adhere to the standard MLLM framework, where the decoder of the MLLM directly outputs the coordinates. Since LLMs are inherently not well-suited for dense prediction tasks, another type of MLLM-based grounding method exists, which focuses on introducing a task-specific decoder. For example, LISA [24] and GLaMM [45] leverages the SAM decoder for pixel-level referring image segmentation while LLaVA-grounding [25] introduces an additional grounding module to predict bounding boxes. Although they have achieved great progress in visual grounding, they still face challenges in precisely aligning coordinates with spatial information in images. Besides, almost all these models are trained on large-scale datasets. For example, MiniGPT-v2 [13] trains on approximately 21M grounding data samples. In contrast, our approach explicitly aids MLLMs in learning these correspondences by providing clear positional references, achieving state-of-the-art performance while requiring training on only a much smaller dataset.

B. Visual Prompt

Visual prompts are used by researchers to guide models in specific tasks [19], [46], [47], as they are more direct than text

prompts [48], [49]. In the Vision-and-Language Pre-training (VLP) models, VPT [50], MaPLe [49], and CMPA [51] add several learnable tokens before the CLIP visual embeddings, transferring CLIP to few-shot classification tasks. PEVL [52] and CPT [53] adapt position-sensitive vision-language tasks like visual grounding to mask token prediction. Recently, visual prompts are introduced in large vision models like SAM [54] and its variants [55], [56] to guide image segmentation. In the field of MLLMs, many works consider the visual prompt approach for specific downstream tasks. [27] and [26] present position-guided visual prompts for GPT-4V, which highly rely on the model's own Chain-of-Thought ability. Ferret [7] and ViP-LLaVA [57] introduce hand-drawn free-form visual prompts, such as scribbles and arrows, for building user-friendly MLLMs. [58] proposes a transferable visual prompt method that can be applied to different models on downstream tasks after training on a single model. [59] suggest incorporating external knowledge, such as segmentation masks as visual prompts for MLLMs, to enhance their visual understanding performance.

III. METHODS

A. Overview

In this section, we present VPP-LLaVA, an MLLM-based method with the Visual Position Prompt for visual grounding. As depicted in Fig. 2, our overall framework follows that of LLaVA-v1.5 [3]. It includes a CLIP-L/336 visual encoder for extracting image features, a 2-layer MLP for mapping these features to the LLM's feature space, and a Vicuna-v1.5 [41] model as the LLM backbone to process the tokenized text prompts. To help MLLMs precisely align coordinates and spatial information within images, we introduce both global and local Visual Position Prompts.

B. Global Visual Position Prompt

Inspired by [26], [58], [27], we introduce a learnable global Visual Position Prompt (VPP) $\delta_g \in \mathbb{R}^{3 \times H \times W}$ to provide a global position reference for the MLLM, initializing it in an axis-like form.

$$\delta_g^i \leftarrow X_{axis} \in \mathbb{R}^{3 \times H \times W}, \quad (1)$$

where δ_g^i is the initialized global VPP and X_{axis} denotes the axes image with coordinate axes along its edges, using a unit scale of 0.1. As shown in Fig. 2, this design aligns with the coordinate data format in LLaVA's training dataset, providing the MLLM with a global reference. In contrast, we avoided adding coordinate axes outside the image, as this would misalign the image coordinates with the annotated data, leading to confusion and poor performance.

The global VPP is overlaid onto input images with standard transformations, such as resizing and padding. Mathematically, the process of the global VPP can be described as follows:

$$X^{gp} = \alpha \cdot \mathcal{T}_v(X) + (1 - \alpha) \cdot \mathcal{T}_{ipt}(\delta_g^i \odot M_w), \quad (2)$$

where α is a trade-off parameter that controls the strength of the overlaid global VPP. $\mathcal{T}_v(\cdot)$ represents the visual encoder's

preprocessing transformations, such as resize and padding in CLIP. \mathcal{T}_{ipt} denotes an interpolation operation that scales the global prompt to fit the size of the processed input. M_w is a binary mask with a width of w around the edges, which we use to control the visible range of the global VPP. Since we initialize the global VPP as an axis-like image with coordinates along its edges, this masking is essential, as not all pixels in it need to be visible.

After we obtain the input image with the added global VPP X_{gp} , we send it to the visual encoder of LLaVA, i.e., CLIP-L/336, to get the image features.

$$F_{gp} = CLIP(X^{gp}), \quad (3)$$

Then, a two-layer MLP, similar to that used in LLaVA, is used to project the image features into the language space of the LLM.

$$F'_{gp} = MLP(F_{gp}), \quad (4)$$

C. Local Visual Position Prompt

To further enhance and incorporate object spatial information, we introduce a local VPP, which serves as a local position reference.

Specifically, in our implementation, we use DETR [15] as our local VPP generator to handle the entire local prompt generation process. Let $\mathcal{O} = \{o_i\}, i = 1\dots k$ denote a set of object queries. By feeding the image with the overlaid global prompt and object queries into DETR's transformer encoder and decoder, we obtain 100 object query embeddings per image, capturing both potential object locations and semantic information.

$$F_{lp} = DETR(X_{gp}, \mathcal{O}), \quad (5)$$

where F_{lp} denotes the generated local Visual Position Prompt, and $DETR(\cdot)$ denotes the DETR model, which includes a ResNet-101 backbone, a 6-layer transformer encoder, and a 6-layer transformer decoder. Following LLaVA, we also use a 2-layer MLP to map the features of the local prompt into the LLM's space.

$$F'_{lp} = MLP(F_{lp}), \quad (6)$$

The proposed local VPP distinguishes itself from other DETR-based methods in two key aspects: First, unlike existing two-stage visual grounding MLLMs that heavily rely on pre-trained detectors to extract bounding box proposals [6], [45], we dynamically generate object position embeddings that capture both spatial and semantic information. This allows the LLM decoder to integrate object-level details more effectively. Second, unlike methods such as ContextDET [60], which incorporate DETR and add an extra box decoder while using the LLM solely for fusion, our method is a pure MLLM. This design not only simplifies the architecture but also enhances performance by enabling a more seamless integration of visual and language modalities.

D. Instruction Tuning and Data Construction

Once the image features from both prompts are obtained, we directly concatenate them and feed the combined features,

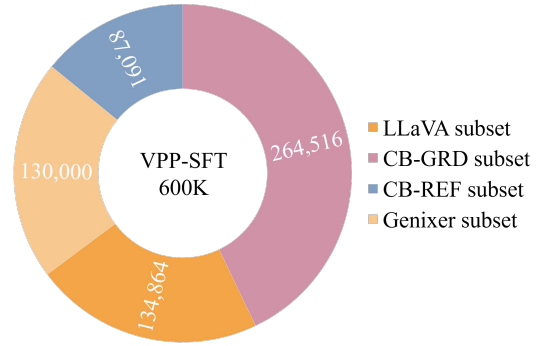


Fig. 3. An overview of our constructed dataset VPP-SFT.

along with the query text instructions, into the LLM for processing. We utilize the pre-trained Vicuna-v1.5 [41] from LLaVA-v1.5 as our LLM. The response is generated by the LLM through autoregressive language modeling, i.e., by maximizing the likelihood of the next token prediction, which can be formulated as follows:

$$P(X_a | F', X_q) = \prod_{i=1}^L P_\theta(x_i | F', X_q, X_{a,< i}), \quad (7)$$

$$F' = \text{concatenate}([F'_{gp}, F'_{lp}]), \quad (8)$$

Here, F' represents the concatenated visual features obtained by applying both the global and local VPP. The symbol θ denotes the parameters of the LLM, X_q stands for the query text instructions, L refers to the sequence length of the answer X_a , and $X_{a,< i}$ encompasses all answer tokens that precede the current prediction token x_i , where i indicates the step in the next word token prediction process.

For instruction tuning of our model, we construct a dataset, VPP-SFT, containing approximately 0.6M samples, significantly smaller than other datasets commonly used for grounding in many MLLMs. For example, MiniGPT-v2 [13] uses 21M grounding samples, KOSMOS-2 [43] uses 20M, and even the relatively smaller Shikra [20] utilizes 4M samples.

As shown in Table 3, our constructed dataset primarily derives from four main sources: a subset of LLaVA-665K [3], CB-GRD [61], CB-REF [61], and Genixer [62], containing 134,864, 264,516, 87,091, and 130,000 conversations, respectively, due to the high quality of their original data. Since our model is built on the pre-trained LLaVA model, we convert all bounding boxes and instructions to follow the format used by LLaVA. Specifically, we adapt the bounding box coordinates to the LLaVA format, pad images along their longer edges, and normalize coordinates in the (x_1, y_1, x_2, y_2) form. To retain LLaVA's original language capabilities, we incorporate a small amount of region-captioning data (e.g., CB-REF subset), formatted with instructions like: *Please provide a short description for this region: xxx*. We aim for the tuned MLLM not only to provide coordinates in response but also to recognize and interpret coordinates as part of the language queries. The combination of these two types of data enhances the model's spatial awareness of object locations in images,

TABLE I

TRAINING DATA EXAMPLES IN THE VPP-SFT DATASET. WE PROVIDE TWO SAMPLES: THE FIRST IS A TRAINING DATA SAMPLE FOR VISUAL GROUNDING, AND THE SECOND IS A REGION CAPTIONING SAMPLE USED TO MAINTAIN THE LANGUAGE CAPABILITIES OF THE MLLM DURING DOWNSTREAM SFT.

User:	<image>\nPlease provide the bounding box coordinate of the region this sentence describes: second cell phone from left. Each image is accompanied by axes. If the question pertains to the bounding box coordinates, refer to the axes for the response.
VPP-LLaVA:	[0.35, 0.64, 0.55, 0.88]
User:	<image>\nPlease provide a short description for this region: [0.44, 0.67, 0.56, 0.83]. Each image is accompanied by axes. If the question pertains to the bounding box coordinates, refer to the axes for the response.
VPP-LLaVA:	It is a black charger.

improving its ability to perceive spatial information. A sample from our dataset is shown in Table I.

It is important to note that VPP-SFT is not just a simple fusion of other datasets. Many MLLM papers introduce fragmented datasets that are hard to reuse. VPP-SFT tries to bring these scattered visual grounding datasets together for MLLMs. Unlike other instruction-tuning datasets for grounding, which often have complex formats with lots of special position tokens, our data format is refreshingly straightforward. This simplicity makes it easier to create new datasets based on ours and allows for more direct fine-tuning of models to boost MLLM spatial awareness. As a result, our dataset is highly reusable and adaptable.

IV. EXPERIMENTS

A. Benchmarks

RefCOCO/RefCOCO+/RefCOCOg. The datasets used in this study are derived from the MSCOCO [63]. RefCOCO contains 50,000 objects across 19,994 images, accompanied by 142,209 expression queries, with each query averaging 3.61 words in length. It is officially divided into training, val, testA, and testB sets, containing 120,624, 10,834, 5,657, and 5,095 expressions, respectively. Split testA focuses on expressions describing people, while testB emphasizes objects other than people. RefCOCO+ features 141,564 expressions for 49,856 objects within 19,992 images. Each query has an average length of 3.53 words. Contrary to RefCOCO, RefCOCO+ prohibits the use of absolute location expressions like *right*, and *top*, thus emphasizing the visual attributes of the referenced objects. The dataset is officially partitioned into training, val, testA, and testB, with 120,191, 10,758, 5,726, and 4,889 expressions, respectively. RefCOCOg features 49,822 objects across 25,799 images with 95,010 expression queries averaging 8.43 words. This dataset is available in two versions: RefCOCOg-google [64] and RefCOCOg-umd [65]. Following the previous studies [13], [7], [66], we report our performance on the RefCOCOg-umd dataset.

ReferIt. To evaluate the transferability of our model’s visual grounding capabilities to other datasets, we conduct zero-shot visual grounding experiments on the ReferIt dataset. This dataset consists of 20,000 annotated images and is notable for containing ambiguous queries (e.g., *any* and *whole*). Besides, some of these samples are labeled with inaccurate bounding boxes. Officially, it is split into three subsets for training,

validation, and testing, which comprise 54,127, 5,842, and 60,103 queries, respectively.

B. Implementation Details

Inputs. For the visual encoder, we follow the same pre-processing steps as LLaVA: padding each image based on its longer side and then applying the CLIP/L-336 processor, which resizes the padded image to 336×336 pixels while preserving the original aspect ratio. For the input to the local VPP generator (DETR-ResNet101 in our model), we resize and pad the images to 640×640 pixels without any additional data augmentations.

Training details. We initialize our model with pre-trained LLaVA-v1.5-7B parameters and fine-tune it using the AdamW optimizer with a cosine annealing scheduler. The learning rates are set as follows: 2e-5 for the LLM (Vicuna-v1.5-7B), 2e-4 for the global VPP, 2e-5 for the local VPP generator, and 2e-4 for the projector that maps the local VPP to the LLM feature space. Unless otherwise specified, our default configuration refers to the 7B model (VPP-LLaVA-7B). Following recent works such as Cambrian-1 [21], Eagle [67], and LLaVA-NeXT [4], which demonstrate that unfreezing the visual encoder is greatly beneficial to vision-centric tasks, we adopt the same strategy, setting the learning rate of the visual encoder to 2e-6. Moreover, following Ferret, we fine-tune our model on the collected VPP-SFT dataset for 3 epochs, and the global batch size is set to 64, which takes roughly 30 hours on 8× NVIDIA A800 GPUs (80GB) for the whole training process. Additionally, the width of the binary mask w and the tradeoff parameter α in Eq. 2 are set to 30 pixels and 0.95 by default, respectively, with more details available in the Section IV-G7.

C. Main Results

In Table II, we report the accuracy performance with an IoU threshold of 0.5 on widely used visual grounding benchmarks [63], [65]: RefCOCO, RefCOCO+, and RefCOCOg. We categorize the compared state-of-the-art models into two types: specialist and generalist models. The methods marked with † indicate that they use ViT-BigG (1.9B) [68] and EVA-G (1.1B) [69] as their visual encoders, respectively, and are significantly larger than CLIP-L/336 used in our model. We also report the scale of the visual grounding data used for training the visual grounding capabilities of these models. From the results, we draw several observations as follows:

TABLE II

COMPARISONS ON VISUAL GROUNDING BENCHMARKS. QWEN-VL-7B AND LION-4B ARE MARKED WITH THE SYMBOL \dagger BECAUSE THEY LEVERAGE A MUCH LARGER VISUAL ENCODER (1.9B ViT-BIGG [68] AND 1.1B EVA-G [69], RESPECTIVELY). THE HIGHEST PERFORMANCE IS MARKED IN BOLD, AND THE SECOND-HIGHEST PERFORMANCE IS MARKED WITH AN UNDERLINE.

Method	Model type	Grounding Data Scale	RefCOCO			RefCOCO+			RefCOCOg	
			val	testA	testB	val	testA	testB	val	test
OFA-L [37]	Specialist	10M	79.96	83.67	76.39	68.29	76.00	61.75	67.57	67.58
TransCP [29]		-	84.25	87.38	79.78	73.07	78.05	63.35	-	-
MDETR [36]		-	86.75	89.58	81.41	79.52	84.09	70.62	81.64	80.89
UNINEXT-L [38]		-	91.43	93.73	88.93	83.09	87.90	76.15	86.91	87.48
KOSMOS-2 [43]	Generalist	20M	52.32	57.42	47.26	45.48	50.73	42.24	60.57	61.65
Shikra-7B [20]		4M	87.01	90.61	80.24	81.60	87.36	72.12	82.27	82.19
Shikra-7B+Genixer [62]		\sim 4.4M	87.48	91.05	81.77	81.89	87.43	73.14	81.99	83.15
Ferret-7B [7]		8.7M	87.49	91.35	82.45	80.78	87.38	73.14	83.93	84.76
GroundingGPT		\sim 2.5M	88.02	91.55	82.47	81.61	87.18	73.18	81.67	81.99
MiniGPT-v2-7B [13]		\sim 21M	88.06	91.29	84.30	79.58	85.52	73.32	84.19	84.31
Qwen-VL-7B [22] \dagger		\sim 21M	88.55	92.27	84.51	82.82	88.59	76.79	<u>85.96</u>	<u>86.32</u>
PINK [44]		5M	88.70	92.10	84.00	81.80	88.20	73.90	83.90	84.30
Groma [6]		\sim 26M	89.53	92.09	86.26	<u>83.90</u>	<u>88.91</u>	78.05	86.37	87.01
VPP-LLaVA-7B		\sim0.6M	90.37	92.89	<u>85.77</u>	84.65	89.84	<u>76.99</u>	85.33	85.52
Shikra-13B [20]	Generalist	4M	87.83	91.11	81.81	82.89	87.79	74.41	82.64	83.16
Ferret-13B [7]		8.7M	89.48	<u>92.41</u>	84.36	82.81	88.14	75.17	<u>85.83</u>	86.34
Griffon-v2-13B [70]		\sim 13M	89.60	91.80	86.50	81.90	85.50	76.20	85.90	86.00
Lion-12B [66] \dagger		7.2M	89.80	93.02	85.57	<u>83.95</u>	<u>89.22</u>	<u>78.06</u>	85.52	85.74
VPP-LLaVA-13B		\sim0.6M	90.32	93.02	<u>86.34</u>	84.65	90.78	79.06	85.64	86.01

Firstly, as a generalist model, our VPP-LLaVA-7B demonstrates strong visual grounding capability, outperforming most of the specialist models. For instance, our method exceeds the performance of OFA-L, TransCP, and MDETR by a substantial margin. Even when compared to the most state-of-the-art specialist model, UNINEXT-L, which is trained on a diverse range of grounding and detection datasets such as object365 and the SOT&VOS datasets, our model surpasses it on the three splits of RefCOCO+ with absolute margins of 2.56%, 1.94%, and 0.84%, respectively.

Secondly, for the RefCOCO dataset, which involves short and position-based expressions averaging 3.6 words, our model achieves the best performance among the group of generalist models compared to others with over 4M grounding data samples. This demonstrates that the introduction of both global and local VPPs is highly effective. These prompts provide position references for MLLMs to locate objects, which facilitates the MLLM's learning and establishment of associations between spatial information and coordinates.

Thirdly, RefCOCO+, which excludes absolute location expressions such as *right*, *top*, and *left*, significantly impacts the grounding achievements of most generalist models. In contrast, our method, leveraging both global and local VPPs, compensates for the lack of absolute location terms and achieves commendable grounding results.

Finally, RefCOCOg, which contains long and more complex queries, is an even more challenging dataset. Despite differences in data scale and visual encoder capabilities, our method

achieves competitive performance on RefCOCOg compared to current state-of-the-art methods such as Qwen-VL-7B and Groma. This phenomenon further demonstrates the effectiveness of our proposed method. By incorporating VPPs, our MLLM can more effectively align spatial information within images to coordinates, even when trained on significantly smaller datasets (0.6M vs. over 20M).

To sum up, the experimental results demonstrate the superiority and effectiveness of our VPP-LLaVA.

D. Scaling Up

To perform a more comprehensive evaluation of the proposed model, we scaled up VPP-LLaVA to 13B settings. We use Vicuna-v1.5-13B, trained with LLaVA-v1.5-13B, as our LLM. The remaining settings are consistent with other configurations mentioned in the Section IV-C. The results are shown in Table II.

For the RefCOCO dataset, despite the limited scale of grounding data used for training, VPP-LLaVA-13B achieves either the best or comparable performance to the top-performing method across all three splits (val, testA, and testB). Moreover, The evaluation results on RefCOCO+ confirm the effectiveness of our approach, showing consistent performance improvements observed in previous experiments. Notably, VPP-LLaVA-13B outperforms Griffon-v2-13B by a significant margin. This improvement likely stems from Griffon-v2-13B's limitations in handling scenarios like RefCOCO+, where absolute positional terms are absent. In con-

TABLE III
TRANSFERABILITY STUDY OF VPP ON LLAVA-NEXT.

Method	RefCOCO			RefCOCO+			RefCOCOg		
	val	testA	testB	val	testA	testB	val	test	
LLaVA-NeXT	84.74	89.67	77.29	77.27	85.71	66.86	80.12	79.68	
LLaVA-NeXT+VPP	90.28	93.26	86.73	84.75	90.48	77.99	85.60	85.53	

TABLE IV
TRANSFERABILITY STUDY OF VPP-LLAVA ON THE REFERIT DATASET IN ZERO-SHOT SETTINGS

Method	ReferIt val	ReferIt test
LLaVA-v1.5-7B	48.95	47.42
VPP-LLaVA-7B	57.55	56.53

trast, our Visual Position Prompts (VPPs) enable VPP-LLaVA-13B to infer positional information effectively, resulting in more accurate bounding box predictions. These findings align with earlier observations.

The results on RefCOCOg are also consistent with the previous experimental results obtained with 7B settings. Even with differences in the visual encoder and training scale, our model still achieves competitive performance against state-of-the-art methods, thereby proving the effectiveness of our proposed approach.

In summary, after scaling up to 13B parameters, VPP-LLaVA consistently maintains its advantages, proving that the enhancements we propose are both scalable and effective.

E. Transferability Studies for VPP

Transferability studies hold two implications for our work: First, whether the proposed VPP can be transferred to models beyond LLava-v1.5 and similarly enhance their visual grounding capabilities; second, whether the proposed VPP-LLaVA can be transferred to other datasets in a zero-shot manner. To address these concerns, we apply the proposed VPP to LLava-NeXT-7B using the main experiment’s training strategy, with results in Table III. Additionally, in Table IV, we present the zero-shot visual grounding test of VPP-LLaVA-7B on the ReferIt dataset.

From Table III, we observe that the proposed VPP method can be transferred to other models, thereby enhancing their visual grounding performance.

From Table IV, it can be observed that compared to LLava-7B, VPP-LLaVA-7B demonstrates a significant improvement in zero-shot visual grounding performance on the ReferIt dataset. Specifically, VPP-LLaVA-7B achieves an accuracy boost of absolutely 8.6% on the ReferIt val split and 9.11% on the ReferIt test split.

F. Results of Region Captioning

The language generation capability of VPP-LLaVA is also evaluated, despite not being the primary focus. Table V shows the results of region captioning on the RefCOCOg dataset. VPP-LLaVA-7B achieves a leading CIDEr score of 73.1, demonstrating comparable performance to larger models. This

TABLE V
COMPARISONS OF REGION CAPTIONING ON REFCOCOG. MODELS MARKED IN GRAY INDICATE THE USE OF LARGER LANGUAGE MODELS. THE HIGHEST PERFORMANCE IS MARKED IN BOLD, AND THE SECOND-HIGHEST PERFORMANCE IS MARKED WITH AN UNDERLINE.

Method	METEOR	BERTScore-F1	CIDEr
GPT4ROI	9.7	87.3	-
Kosmos-2	12.2	<u>87.1</u>	60.3
LLaVA-v1.5-7B	12.0	86.9	73.1
Griffon-v2-13B	12.1	-	72.5
ChatterBox-13B	14.5	88.0	-
VPP-LLaVA-7B	<u>12.1</u>	<u>87.1</u>	73.1

highlights its efficiency and ability to generate semantically rich captions. Despite its 7B parameter size and limited training data, it matches or even outperforms some 13B models in key metrics, showcasing its competitive strength. However, its METEOR score of 12.1 indicates potential room for improvement in caption accuracy. For other MLLMs, as seen in many published works such as Groma, LISA, and Griffon, general language capabilities are often compromised due to the size and type of the SFT datasets. This remains a significant challenge in the MLLM field, which we leave for future work.

G. Ablation Study

To conserve time and computational resources, we freeze the visual encoder (except in Section IV-G6) and randomly select 150K samples from VPP-SFT to form our ablation training set. All subsequent ablation results are based on this subset and are specific to the VPP-LLaVA-7B model.

1) *Components*: Table VI shows VPP-LLava’s performance with different components on grounding benchmarks. Without the proposed VPP, the model degrades to LLava-v1.5 (the baseline, which is also trained on the same 150K subset with the same training strategy as described earlier for fairness). Adding the global VPP improves baseline performance across datasets, especially on RefCOCOg, with a 1.5% gain, highlighting its effectiveness in providing a reliable spatial reference. The local VPP alone shows mixed results, sometimes comparable to or slightly below baseline, likely due to limited data hindering effective DETR feature alignment. However, combining global and local VPPs yields a synergistic effect, enhancing grounding accuracy by around 2% on RefCOCO testB, as the global reference supports overall spatial orientation while the local VPP contributes region-specific semantic cues, jointly boosting performance.

2) *Impact of Trainable Global VPP*: In our approach, the default setting allows the global VPP to be trainable. It is essential to examine the impact of training versus not training the global VPP. To conserve time and computational resources, we maintain the same setup as in our previous ablation study, using a 150K subset sampled from VPP-SFT while keeping CLIP frozen. The results are presented in Table VII. We can observe that making the global VPP learnable is beneficial. This is because the pixel values of the axis-like images we

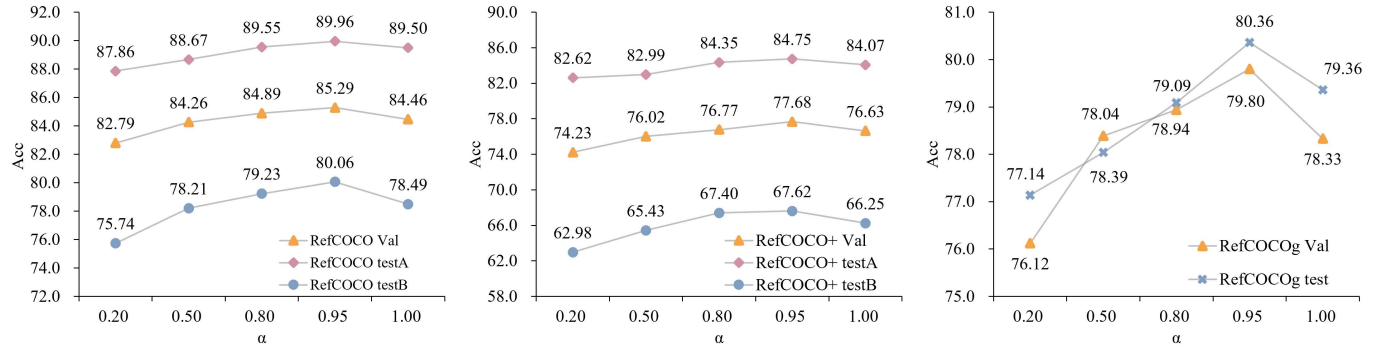


Fig. 4. The ablation study of the trade-off parameter α in global VPP. The left, middle, and right figures present results on RefCOCO, RefCOCO+, and RefCOCOg, respectively. Overall, the performance indicates that $\alpha = 0.95$ achieves the best results.

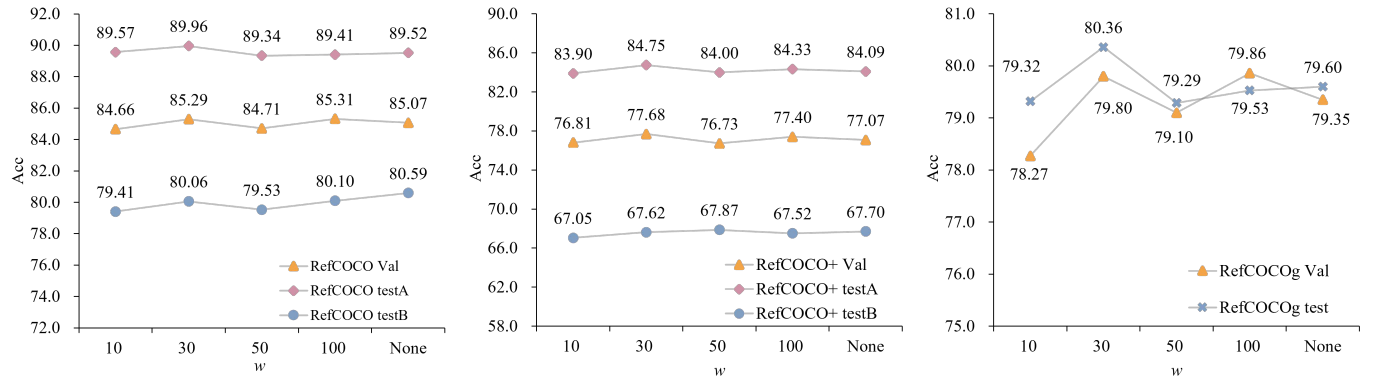


Fig. 5. The ablation study of the width w of the binary mask M_w in global VPP. The left, middle, and right figures present results on RefCOCO, RefCOCO+, and RefCOCOg, respectively. Overall, the performance indicates that $M_w = 30$ pixels achieves the best results.

TABLE VI
THE ABLATION STUDY OF DIFFERENT MODULES IN OUR PROPOSED METHOD.

Global VPP	Local VPP	RefCOCO				RefCOCO+				RefCOCOg			
		val	testA	testB	val	testA	testB	val	testA	testB	val	test	val
✓	✓	84.58	89.62	78.07	77.04	83.79	67.00	78.23	78.63	79.27	79.79	79.33	79.36
		84.95	89.87	78.78	77.20	84.30	67.27	79.27	79.79	79.53	79.86	79.86	80.36
✓	✓	84.46	89.50	78.49	76.63	84.07	66.25	78.33	79.36	79.53	79.86	79.86	80.36
✓		85.29	89.96	80.06	77.68	84.75	67.62	79.80	80.36	(+0.71)	(+0.34)	(+1.99)	(+0.64)

TABLE VII

THE ABLATION STUDY OF THE IMPACT ABOUT THE GLOBAL VPP BEING TRAINABLE OR NON-TRAINABLE.

Trainable	RefCOCO			RefCOCO+			RefCOCOg		
	val	testA	testB	val	testA	testB	val	test	val
✗	84.77	89.57	79.27	77.04	83.43	67.11	79.04	79.88	
✓	85.29	89.96	80.06	77.68	84.75	67.62	79.80	80.36	

use for initialization may not be suitable for every image. By making it learnable, the model can dynamically adapt to different inputs, thereby achieving better performance.

3) *Variants of Global VPP Initialization:* The Global VPP is initialized by default with an axes image that features

TABLE VIII
THE ABLATION STUDY ON VARIANTS OF GLOBAL VPP INITIALIZATION.

Type	RefCOCO			RefCOCO+			RefCOCOg		
	val	testA	testB	val	testA	testB	val	test	val
Interval-0.05	84.62	88.76	79.63	76.83	84.09	67.43	79.15	79.49	
Cross-axis-0.1	84.68	88.49	78.88	77.55	83.60	66.56	78.64	79.96	
Default	85.29	89.96	80.06	77.68	84.75	67.62	79.80	80.36	

coordinate axes along its edges, using a unit scale of 0.1. To evaluate how different initial axes images affect the grounding performance of the model, we conduct experiments under two distinct conditions: one with a unit scale of 0.05 and axes along the edges (Interval-0.05 in Table VIII), and another

TABLE IX

THE ABLATION STUDY OF DIFFERENT TYPES OF LOCAL VPP GENERATOR.
A.DETR AND V.DETR ARE THE ABBREVIATION FOR ANCHOR-DETR
AND VANILLA-DETR RESPECTIVELY.

Type	RefCOCO			RefCOCO+			RefCOCOg		
	val	testA	testB	val	testA	testB	val	test	
A. DETR	84.21	89.22	79.21	76.00	84.19	86.01	78.76	79.38	
V. DETR	85.29	89.96	80.06	77.68	84.75	67.62	79.80	80.36	

TABLE X

THE ABLATION STUDY OF THE FUSION STRATEGY. C.A.1, C.A.2 AND Cat. ARE THE ABBREVIATION FOR CROSS-ATTENTION-1, CROSS-ATTENTION-2, AND CONCATENATE OPERATION RESPECTIVELY.

Strategy	RefCOCO			RefCOCO+			RefCOCOg		
	val	testA	testB	val	testA	testB	val	test	
C.A.1	40.37	43.15	34.34	26.34	30.20	21.47	29.98	29.94	
C.A.2	82.74	86.97	76.94	73.71	80.49	63.37	76.33	76.42	
Cat.	85.29	89.96	80.06	77.68	84.75	67.62	79.80	80.36	

with a unit scale of 0.1 and cross axes centered at the image (Cross-axis-0.1 in Table VIII). It should be noted that when the cross axes are equipped, the binary mask needs to be removed. The results show that the default settings that the global VPP around all edges with the 0.1 unit scale, as used in our paper, performs better. Furthermore, the interval should be based on the internal coordinate system of the MLLM base model due to differences among MLLMs. We will explore more initialization forms in the future.

4) *Type of Local VPP Generator:* We compare the performance of using different types of DETR to obtain the local VPP, including anchor-DETR (A.DETR) [16] and vanilla-DETR (V.DETR) [15]. As shown in Table IX, A.DETR is generally inferior to V.DETR. This may be due to the excessive number of object queries (900 for A.DETR and 100 for V.DETR) interfering with the LLM’s judgment. Furthermore, it remains to be investigated in future work whether a more powerful DETR variant could improve visual grounding performance.

5) *Fusion Strategy:* Table X presents our ablation study on fusion strategies for combining F'_{gp} (CLIP visual features with global VPP) and F'_{lp} (features from the local VPP generator) as outlined in Eq. 8. Here, C.A.1 stands for *cross-attention-1*, which uses F'_{lp} as the query and F'_{gp} as the key in cross-attention, while C.A.2 reverses this, using F'_{gp} as the query and F'_{lp} as the key. Cat. denotes direct concatenation. The cross-attention modules, trained with a learning rate of 2e-4, underperform relative to simple concatenation. This may be due to their training from scratch, which limits alignment with the LLM’s pre-trained representations. Consequently, we adopt direct concatenation for our final model.

6) *Freeze or Unfreeze Visual Encoder:* In Table XI, we report the results of freezing versus unfreezing the MLLM’s visual encoder in our models. We observe that unfreezing the visual encoder significantly enhances performance on down-

TABLE XI

THE ABLATION STUDY EXAMINES WHETHER TO FREEZE OR UNFREEZE THE VISUAL ENCODER.

Unfreeze	RefCOCO			RefCOCO+			RefCOCOg		
	val	testA	testB	val	testA	testB	val	test	
\times	85.29	89.96	80.06	77.68	84.75	67.62	79.80	80.36	
\checkmark	86.48	91.25	81.59	79.75	86.22	70.38	81.14	82.14	

stream visual grounding task. Since the introduced global VPP does not naturally exist in the MLLM’s pretraining dataset, unfreezing the visual encoder allows it to better learn and adapt to this new form of input. This observation is also supported by recent research [21], [67], [4].

7) *Hyperparameters:* In our proposed VPP method, the key hyperparameters are the trade-off parameter α and the width w of the binary mask M_w (Eq. 2). Specifically, α controls the strength of the global VPP overlay, while M_w defines its visible range. The impact of these hyperparameters on visual grounding performance is shown in Fig. 4 and Fig. 5.

As shown in Fig. 4, performance is optimal when α is set to 0.95 across all datasets. A smaller α reduces the visibility of the MLLM’s visual features, leading to lower performance. As α increases, allowing greater visibility of the original MLLM features, grounding performance improves. However, when α reaches 1 (no global VPP), performance declines, suggesting that excessive transparency negatively impacts the model. Thus, the global VPP should enhance rather than overpower the original visual features.

For the binary mask width w , as shown in Fig. 5. The default width of 30 (used for initializing axis-like images, as shown in Fig. 2) yields the best performance. Both overly small ($w = 10$) and overly large ($w = \text{None}$, no mask) values hinder performance. A small w limits the visibility of the coordinate axes, reducing the effectiveness of the global VPP, while a large w introduces excessive distortion, negatively impacting the visual features. Therefore, a balanced mask width is crucial for optimal performance.

V. QUALITATIVE RESULTS

A. Qualitative Dialogue

To fully understand the position-enhanced VPP-LLaVA for grounding tasks, we present our qualitative dialogue in Fig. 6. The predicted bounding box is marked in red, and the ground truth is marked in green. For brevity, some instruction prompts are omitted, and the full form of the conversation can be found in Table I. Specifically, cases (a), (b), and (c) are three visual grounding examples from RefCOCO, RefCOCO+, and RefCOCOg, respectively. We can observe that our VPP-LLaVA demonstrates strong visual grounding capacity on these widely used benchmarks through the proposed global and local VPP.

Furthermore, to demonstrate that our model retains satisfactory language capabilities after fine-tuning for visual grounding, we present two region captioning results on the RefCOCOg dataset in cases (d), (e) and (f). For ease of

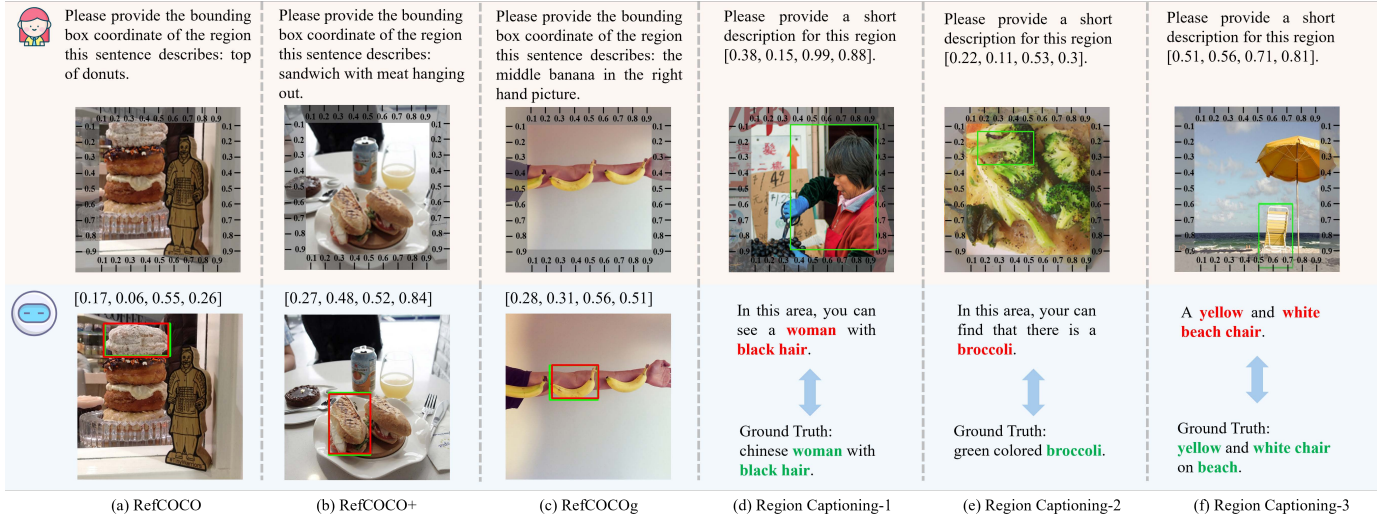


Fig. 6. Qualitative results of our VPP-LLaVA on visual grounding and region captioning tasks. For brevity, some text instructions are omitted. **Green:** ground truth; **Red:** ours.



Fig. 7. Qualitative visual grounding results of our VPP-LLaVA compared with the state-of-the-art method MiniGPT-v2 on RefCOCO dataset. For brevity, some text instructions are omitted. **Green:** ground truth; **Red:** ours; **Brown:** MiniGPT-v2.

understanding, we mark the ground truth bounding boxes and the language phrases in these cases. We find that VPP-LLaVA accurately identifies the given regions and provides essentially correct captions. For example, in the final case of Fig. 6, our model accurately understands the given coordinates and outputs a suitable text response that includes the beach chair, along with its fine-grained attributes: yellow and white.

Overall, it is evident that the introduction of VPPs effectively assists the model in aligning spatial information in the images with coordinates, thereby enabling a better understanding of the images.

B. Qualitative Comparisons

Additional qualitative results for visual grounding are presented in Fig. 7. Here, the green, red, and brown colors correspond to the bounding boxes of the ground truth, our VPP-LLaVA, and miniGPT-v2, respectively. For simplicity, we omit the 7B label in subsequent annotations.

Compared to the MiniGPT-v2 method, VPP-LLaVA demonstrates enhanced accuracy and reliability. For instance, in complex scenarios where the visibility of the target object is limited, as seen in Fig. 7 (b), (c), and (d), VPP-LLaVA accurately identifies the target object, while MiniGPT-v2 struggles. Similar situations can be observed in case (j) and case (l).

Leveraging the global VPP, our method offers superior

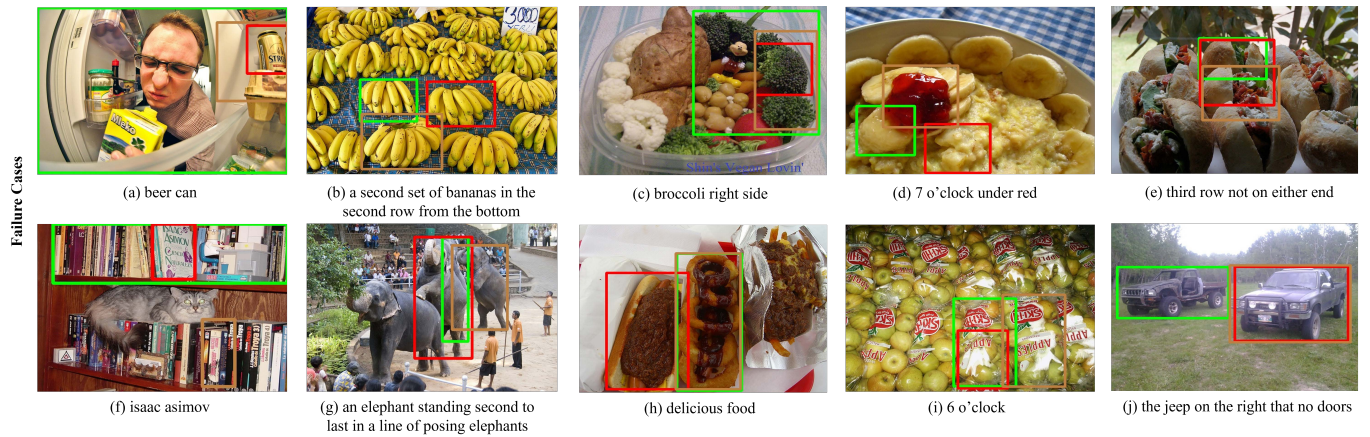


Fig. 8. Some failure cases on visual grounding testing datasets. For brevity, some text instructions are omitted. Green: ground truth; Red: ours; Brown: MiniGPT-v2.

global positional references when the query lacks explicit subject localization. This capability is particularly beneficial in scenarios where the absolute location of the query is not clearly indicated, allowing our approach to perform more effectively. Cases (e), (g), (h), and (i) illustrate this point clearly.

Furthermore, by incorporating local VPP, VPP-LLaVA offers enhanced object potential location and semantic information. This improvement enables the model to more easily distinguish between objects of similar categories. For instance, in case (m), VPP-LLaVA accurately identifies the double-decker bus, whereas the MiniGPT-v2 incorrectly locates a nearby bus. Similar situations can also be found in cases (n) and (o).

C. Failure Cases Study

To provide a comprehensive analysis of VPP-LLaVA, we present several failure cases from the involved datasets in Fig. 8. For clarity, the 7B label is omitted in subsequent annotations. When comparing with the ground truth and MiniGPT-v2, several key observations can be made:

First, in some instances, the ground truth annotations are not entirely accurate. For example, in cases (a) and (f), our method demonstrates its capability to provide a more precise location for the queried object than ground truth annotations. This demonstrates the effectiveness of our proposed VPPs, which allow the model to align image spatial information with coordinate details more accurately, thereby improving visual grounding performance.

Second, both VPP-LLaVA and MiniGPT-v2 may struggle to provide accurate bounding boxes for queries involving complex relational reasoning. Such scenarios remain challenging even for MLLMs with advanced reasoning capabilities. This limitation is evident in cases (b) and (g), where the relationships between objects are particularly intricate.

Third, ambiguous queries that could refer to multiple areas within an image pose significant challenges for both methods. This misalignment is particularly evident in cases (c) and (h), where the ambiguity of the query poses a significant challenge. The situation becomes even more complex when the subject

is missing, as seen in cases (d) and (i), significantly increasing the difficulty of accurate visual grounding.

Lastly, for queries involving negations, such as in cases (e) and (j), both our method and MiniGPT-v2 may exhibit suboptimal performance. This is likely due to ongoing challenges in semantic understanding and reasoning related to negation for MLLMs, as negation requires deeper language comprehension and the ability to infer excluded information.

VI. CONCLUSION

In this paper, we propose VPP-LLaVA, an MLLM-based framework for visual grounding that incorporates the Visual Position Prompt (VPP). The global VPP initializes in an axis-like form and directly overlays onto the input image, providing a foundational position reference for the model. Additionally, the local VPP, serving as a local position reference, provides potential object locations and semantic information. Through these prompts, MLLMs can more accurately align image spatial information with coordinate details, thereby improving the visual grounding performance. Experiments indicate that, even when trained on limited data, our method outperforms state-of-the-art methods on widely used visual grounding benchmarks, demonstrating the superiority of our approach.

REFERENCES

- [1] Y. Li, B. Hu, X. Chen, L. Ma, Y. Xu, and M. Zhang, “Lmeye: An interactive perception network for large language models,” *IEEE Trans. Multimedia*, vol. 26, pp. 10 952–10 964, 2024.
- [2] H. Liu, C. Li, Q. Wu, and Y. J. Lee, “Visual instruction tuning,” in *Proceedings of Advances in Neural Information Processing Systems*, vol. 36, 2024.
- [3] H. Liu, C. Li, Y. Li, and Y. J. Lee, “Improved baselines with visual instruction tuning,” in *Proceedings of the IEEE/CVF Conference on Computer Vision and Pattern Recognition*, 2024, pp. 26 296–26 306.
- [4] H. Liu, C. Li, Y. Li, B. Li, Y. Zhang, S. Shen, and Y. J. Lee, “Llava-next: Improved reasoning, ocr, and world knowledge,” January 2024. [Online]. Available: <https://llava-vl.github.io/blog/2024-01-30-llava-next/>
- [5] Y. Sun, J. Hao, K. Zhu, J.-J. Liu, Y. Zhao, X. Li, G. Zhang, Z. Li, and J. Wang, “Descriptive caption enhancement with visual specialists for multi-modal perception,” *arXiv preprint arXiv:2412.14233*, 2025.
- [6] C. Ma, Y. Jiang, J. Wu, Z. Yuan, and X. Qi, “Groma: Localized visual tokenization for grounding multi-modal large language models,” in *Proceedings of European Conference on Computer Vision*, 2025, pp. 417–435.

- [7] H. You, H. Zhang, Z. Gan, X. Du, B. Zhang, Z. Wang, L. Cao, S. Chang, and Y. Yang, "Ferret: Refer and ground anything anywhere at any granularity," in *Proceedings of the International Conference on Learning Representations*, 2024.
- [8] G. Cong, L. Li, Z. Liu, Y. Tu, W. Qin, S. Zhang, C. Yan, W. Wang, and B. Jiang, "LS-GAN: iterative language-based image manipulation via long and short term consistency reasoning," in *Proceedings of ACM Int. Conf. Multimedia*, 2022, pp. 4496–4504.
- [9] Y. Tu, L. Li, L. Su, Z. Zha, and Q. Huang, "SMART: syntax-calibrated multi-aspect relation transformer for change captioning," *IEEE Trans. Pattern Anal. Mach. Intell.*, vol. 46, no. 7, pp. 4926–4943, 2024.
- [10] Y. Bu, X. Wu, Y. Cai, Q. Liu, T. Wang, and Q. Huang, "Error-aware generative reasoning for zero-shot visual grounding," *IEEE Trans. Multimedia*, 2025.
- [11] M. Xie, M. Wang, H. Li, Y. Zhang, D. Tao, and Z. Yu, "Phrase decoupling cross-modal hierarchical matching and progressive position correction for visual grounding," *IEEE Trans. Multimedia*, 2025.
- [12] L. Xiao, X. Yang, F. Peng, M. Yan, Y. Wang, and C. Xu, "CLIP-VG: self-paced curriculum adapting of CLIP for visual grounding," *IEEE Trans. Multimedia*, vol. 26, pp. 4334–4347, 2024.
- [13] J. Chen, D. Zhu, X. Shen, X. Li, Z. Liu, P. Zhang, R. Krishnamoorthi, V. Chandra, Y. Xiong, and M. Elhoseiny, "Minigpt-v2: Large language model as a unified interface for vision-language multi-task learning," *arXiv preprint arXiv:2310.09478*, 2023.
- [14] H. Tang, Z. Li, D. Zhang, S. He, and J. Tang, "Divide-and-conquer: confluent triple-flow network for RGB-T salient object detection," *IEEE Trans. Pattern Anal. Mach. Intell.*, vol. 47, no. 3, pp. 1958–1974, 2025.
- [15] N. Carion, F. Massa, G. Synnaeve, N. Usunier, A. Kirillov, and S. Zagoruyko, "End-to-end object detection with transformers," in *Proceedings of European Conference on Computer Vision*, 2020, pp. 213–229.
- [16] Y. Wang, X. Zhang, T. Yang, and J. Sun, "Anchor detr: Query design for transformer-based detector," in *Proceedings of the AAAI conference on artificial intelligence*, vol. 36, no. 3, 2022, pp. 2567–2575.
- [17] Z. Li, Y. Sun, L. Zhang, and J. Tang, "Ctnet: context-based tandem network for semantic segmentation," *IEEE Trans. Pattern Anal. Mach. Intell.*, vol. 44, no. 12, pp. 9904–9917, 2022.
- [18] Y. Zhan, Z. Xiong, and Y. Yuan, "Rsvg: Exploring data and models for visual grounding on remote sensing data," *IEEE Trans. Geosci. Remote Sens.*, vol. 61, pp. 1–13, 2023.
- [19] S.-F. Chen, J.-C. Chen, I.-H. Jhuo, and Y.-Y. Lin, "Improving visual object tracking through visual prompting," *IEEE Trans. Multimedia*, pp. 1–12, 2025.
- [20] K. Chen, Z. Zhang, W. Zeng, R. Zhang, F. Zhu, and R. Zhao, "Shikra: Unleashing multimodal llm's referential dialogue magic," *arXiv preprint arXiv:2306.15195*, 2023.
- [21] P. Tong, E. Brown, P. Wu, S. Woo, A. Iyer, S. C. Akula, S. Yang, J. Yang, M. Middepogu, Z. Wang, X. Pan, R. Fergus, Y. LeCun, and S. Xie, "Cambrian-1: A fully open, vision-centric exploration of multimodal llms," in *Proceedings of Advances in Neural Information Processing Systems*, 2024.
- [22] J. Bai, S. Bai, S. Yang, S. Wang, S. Tan, P. Wang, J. Lin, C. Zhou, and J. Zhou, "Qwen-vl: A frontier large vision-language model with versatile abilities," *arXiv preprint arXiv:2308.12966*, 2023.
- [23] Y. Sun, H. Zhang, Q. Chen, X. Zhang, N. Sang, G. Zhang, J. Wang, and Z. Li, "Improving multi-modal large language model through boosting vision capabilities," *arXiv preprint arXiv:2410.13733*, 2024.
- [24] X. Lai, Z. Tian, Y. Chen, Y. Li, Y. Yuan, S. Liu, and J. Jia, "Lisa: Reasoning segmentation via large language model," in *Proceedings of the IEEE/CVF Conference on Computer Vision and Pattern Recognition*, 2024, pp. 9579–9589.
- [25] H. Zhang, H. Li, F. Li, T. Ren, X. Zou, S. Liu, S. Huang, J. Gao, C. Li, J. Yang *et al.*, "Llava-grounding: Grounded visual chat with large multi-modal models," in *Proceedings of European Conference on Computer Vision*, 2025, pp. 19–35.
- [26] Y. Wu, Y. Wang, S. Tang, W. Wu, T. He, W. Ouyang, P. Torr, and J. Wu, "Dettolchain: A new prompting paradigm to unleash detection ability of mllm," in *Proceedings of European Conference on Computer Vision*, vol. 15090, 2024, pp. 164–182.
- [27] X. Lei, Z. Yang, X. Chen, P. Li, and Y. Liu, "Scaffolding coordinates to promote vision-language coordination in large multi-modal models," in *Proceedings of International Conference on Computational Linguistics*, 2025, pp. 2886–2903.
- [28] C. Wang, W. Feng, S. Lyu, G. Cheng, X. Li, B. Liu, and Q. Zhao, "A masked reference token supervision-based iterative visual-language framework for robust visual grounding," *IEEE Trans. Circuits Syst. Video Technol.*, vol. 35, no. 1, pp. 75–90, 2025.
- [29] W. Tang, L. Li, X. Liu, L. Jin, J. Tang, and Z. Li, "Context disentangling and prototype inheriting for robust visual grounding," *IEEE Trans. Pattern Anal. Mach. Intell.*, vol. 46, no. 5, pp. 3213–3229, 2024.
- [30] X. Liu, L. Li, S. Wang, Z.-J. Zha, Z. Li, Q. Tian, and Q. Huang, "Entity-enhanced adaptive reconstruction network for weakly supervised referring expression grounding," *IEEE Trans. Pattern Anal. Mach. Intell.*, vol. 45, no. 3, pp. 3003–3018, 2023.
- [31] L. Yu, Z. Lin, X. Shen, J. Yang, X. Lu, M. Bansal, and T. L. Berg, "Mattnet: Modular attention network for referring expression comprehension," in *Proceedings of IEEE/CVF Conference on Computer Vision and Pattern Recognition*, 2018, pp. 1307–1315.
- [32] M. Sun, J. Xiao, E. G. Lim, and Y. Zhao, "Cycle-free weakly referring expression grounding with self-paced learning," *IEEE Trans. Multimedia*, vol. 25, pp. 1611–1621, 2023.
- [33] Z. Yang, B. Gong, L. Wang, W. Huang, D. Yu, and J. Luo, "A fast and accurate one-stage approach to visual grounding," in *Proceedings of the IEEE/CVF International Conference on Computer Vision*, 2019, pp. 4683–4693.
- [34] Y. Liao, A. Zhang, Z. Chen, T. Hui, and S. Liu, "Progressive language-customized visual feature learning for one-stage visual grounding," *IEEE Trans. Image Process.*, vol. 31, pp. 4266–4277, 2022.
- [35] L. Yang, Y. Xu, C. Yuan, W. Liu, B. Li, and W. Hu, "Improving visual grounding with visual-linguistic verification and iterative reasoning," in *Proceedings of the IEEE/CVF Conference on Computer Vision and Pattern Recognition*, 2022, pp. 9499–9508.
- [36] A. Kamath, M. Singh, Y. LeCun, G. Synnaeve, I. Misra, and N. Carion, "Mdetr: Modulated detection for end-to-end multi-modal understanding," in *Proceedings of the IEEE/CVF International Conference on Computer Vision*, 2021, pp. 1760–1770.
- [37] P. Wang, A. Yang, R. Men, J. Lin, S. Bai, Z. Li, J. Ma, C. Zhou, J. Zhou, and H. Yang, "Ofa: Unifying architectures, tasks, and modalities through a simple sequence-to-sequence learning framework," in *Proceedings of International Conference on Machine Learning*, 2022, pp. 23 318–23 340.
- [38] B. Yan, Y. Jiang, J. Wu, D. Wang, P. Luo, Z. Yuan, and H. Lu, "Universal instance perception as object discovery and retrieval," in *Proceedings of the IEEE/CVF Conference on Computer Vision and Pattern Recognition*, 2023, pp. 15 325–15 336.
- [39] J. Deng, Z. Yang, T. Chen, W. Zhou, and H. Li, "Transvg: End-to-end visual grounding with transformers," in *Proceedings of the IEEE/CVF International Conference on Computer Vision*, 2021, pp. 1769–1779.
- [40] H. Touvron, T. Lavril, G. Izacard, X. Martinet, M.-A. Lachaux, T. Lacroix, B. Rozière, N. Goyal, E. Hambro, F. Azhar *et al.*, "Llama: Open and efficient foundation language models," *arXiv preprint arXiv:2302.13971*, 2023.
- [41] W.-L. Chiang, Z. Li, Z. Lin, Y. Sheng, Z. Wu, H. Zhang, L. Zheng, S. Zhuang, Y. Zhuang, J. E. Gonzalez, I. Stoica, and E. P. Xing, "Vicuna: An open-source chatbot impressing gpt-4 with 90%* chatgpt quality," March 2023. [Online]. Available: <https://lmsys.org/blog/2023-03-30-vicuna/>
- [42] D. Zhu, J. Chen, X. Shen, X. Li, and M. Elhoseiny, "Minigpt-4: Enhancing vision-language understanding with advanced large language models," in *Proceedings of the International Conference on Learning Representations*, 2024.
- [43] Z. Peng, W. Wang, L. Dong, Y. Hao, S. Huang, S. Ma, and F. Wei, "Kosmos-2: Grounding multimodal large language models to the world," *arXiv preprint arXiv:2306.14824*, 2023.
- [44] S. Xuan, Q. Guo, M. Yang, and S. Zhang, "Pink: Unveiling the power of referential comprehension for multi-modal llms," in *Proceedings of the IEEE/CVF Conference on Computer Vision and Pattern Recognition*, 2024, pp. 13 838–13 848.
- [45] H. Rasheed, M. Maaz, S. Shaji, A. Shaker, S. Khan, H. Cholakkal, R. M. Anwer, E. Xing, M.-H. Yang, and F. S. Khan, "Glamm: Pixel grounding large multi-modal model," in *Proceedings of the IEEE/CVF Conference on Computer Vision and Pattern Recognition*, 2024, pp. 13 009–13 018.
- [46] K. Sofiuk, I. Petrov, O. Barinova, and A. Konushin, "f-brs: Rethinking backpropagating refinement for interactive segmentation," in *Proceedings of the IEEE/CVF Conference on Computer Vision and Pattern Recognition*, 2020, pp. 8623–8632.
- [47] Y. Long, J. Han, R. Huang, H. Xu, Y. Zhu, C. Xu, and X. Liang, "Fine-grained visual-text prompt-driven self-training for open-vocabulary object detection," *IEEE Trans. Neural Networks Learn. Syst.*, vol. 35, no. 11, pp. 16 277–16 287, 2024.
- [48] X. Liu, J. Wu, W. Yang, X. Zhou, and T. Zhang, "Multi-modal attribute prompting for vision-language models," *IEEE Trans. Circuits Syst. Video Technol.*, vol. 34, no. 11, pp. 11 579–11 591, 2024.

- [49] M. U. Khattak, H. Rasheed, M. Maaz, S. Khan, and F. S. Khan, “Maple: Multi-modal prompt learning,” in *Proceedings of the IEEE/CVF Conference on Computer Vision and Pattern Recognition*, 2023, pp. 19 113–19 122.
- [50] M. Jia, L. Tang, B.-C. Chen, C. Cardie, S. Belongie, B. Hariharan, and S.-N. Lim, “Visual prompt tuning,” in *Proceedings of European Conference on Computer Vision*, 2022, pp. 709–727.
- [51] X. Liu, W. Tang, J. Lu, R. Zhao, Z. Guo, and F. Tan, “Deeply coupled cross-modal prompt learning,” in *Findings of the Association for Computational Linguistics*, 2023, pp. 7957–7970.
- [52] Y. Yao, Q. Chen, A. Zhang, W. Ji, Z. Liu, T.-S. Chua, and M. Sun, “Pevl: Position-enhanced pre-training and prompt tuning for vision-language models,” in *Proceedings of Conference on Empirical Methods in Natural Language Processing*, 2022, pp. 11 104–11 117.
- [53] Y. Yao, A. Zhang, Z. Zhang, Z. Liu, T. Chua, and M. Sun, “Cpt: Colorful prompt tuning for pre-trained vision-language models,” *AI Open*, vol. 5, pp. 30–38, 2024.
- [54] A. Kirillov, E. Mintun, N. Ravi, H. Mao, C. Rolland, L. Gustafson, T. Xiao, S. Whitehead, A. C. Berg, W.-Y. Lo *et al.*, “Segment anything,” in *Proceedings of the IEEE/CVF International Conference on Computer Vision*, 2023, pp. 4015–4026.
- [55] Y. Sun, J. Chen, S. Zhang, X. Zhang, Q. Chen, G. Zhang, E. Ding, J. Wang, and Z. Li, “Vrp-sam: Sam with visual reference prompt,” in *Proceedings of IEEE/CVF Conference on Computer Vision and Pattern Recognition*, 2024.
- [56] L. Yang, Y. Wang, X. Li, X. Wang, and J. Yang, “Fine-grained visual prompting,” in *Proceedings of Advances in Neural Information Processing Systems*, vol. 36, 2024.
- [57] M. Cai, H. Liu, S. K. Mustikovela, G. P. Meyer, Y. Chai, D. Park, and Y. J. Lee, “Vip-llava: Making large multi-modal models understand arbitrary visual prompts,” in *Proceedings of the IEEE/CVF Conference on Computer Vision and Pattern Recognition*, 2024, pp. 12 914–12 923.
- [58] Y. Zhang, Y. Dong, S. Zhang, T. Min, H. Su, and J. Zhu, “Exploring the transferability of visual prompting for multi-modal large language models,” in *Proceedings of the IEEE/CVF Conference on Computer Vision and Pattern Recognition*, 2024, pp. 26 562–26 572.
- [59] Y. Lin, Y. Li, D. Chen, W. Xu, R. Clark, P. Torr, and L. Yuan, “Rethinking visual prompting for multi-modal large language models with external knowledge,” *arXiv preprint arXiv:2407.04681*, 2024.
- [60] N. Wang, Y. Xiao, X. Peng, X. Chang, X. Wang, and D. Fang, “Contextdet: Temporal action detection with adaptive context aggregation,” *arXiv preprint arXiv:2410.15279*, 2024.
- [61] P. Mavridis, O. Huang, S. Qiu, U. Gadiraaju, and A. Bozzon, “Chatterbox: Conversational interfaces for microtask crowdsourcing,” in *Proceedings of ACM Conference on User Modeling, Adaptation and Personalization*, 2019, pp. 243–251.
- [62] H. H. Zhao, P. Zhou, and M. Z. Shou, “GENIXER: empowering multimodal large language model as a powerful data generator,” in *Proceedings of European Conference on Computer Vision*, vol. 15081, 2024, pp. 129–147.
- [63] T.-Y. Lin, M. Maire, S. Belongie, J. Hays, P. Perona, D. Ramanan, P. Dollár, and C. L. Zitnick, “Microsoft coco: Common objects in context,” in *Proceedings of European Conference on Computer Vision*, 2014, pp. 740–755.
- [64] J. Mao, J. Huang, A. Toshev, O. Camburu, A. L. Yuille, and K. Murphy, “Generation and comprehension of unambiguous object descriptions,” in *Proceedings of IEEE/CVF International Conference on Computer Vision*, 2016, pp. 11–20.
- [65] V. K. Nagaraja, V. I. Morariu, and L. S. Davis, “Modeling context between objects for referring expression understanding,” in *Proceedings of European Conference on Computer Vision*, 2016, pp. 792–807.
- [66] G. Chen, L. Shen, R. Shao, X. Deng, and L. Nie, “Lion: Empowering multimodal large language model with dual-level visual knowledge,” in *Proceedings of the IEEE/CVF Conference on Computer Vision and Pattern Recognition*, 2024, pp. 26 540–26 550.
- [67] M. Shi, F. Liu, S. Wang, S. Liao, S. Radhakrishnan, D.-A. Huang, H. Yin, K. Sapra, Y. Yacoob, H. Shi *et al.*, “Eagle: Exploring the design space for multimodal llms with mixture of encoders,” *arXiv preprint arXiv:2408.15998*, 2024.
- [68] X. Zhai, A. Kolesnikov, N. Houlsby, and L. Beyer, “Scaling vision transformers,” in *Proceedings of the IEEE/CVF conference on computer vision and pattern recognition*, 2022, pp. 12 104–12 113.
- [69] Y. Fang, W. Wang, B. Xie, Q. Sun, L. Wu, X. Wang, T. Huang, X. Wang, and Y. Cao, “Eva: Exploring the limits of masked visual representation learning at scale,” in *Proceedings of the IEEE/CVF Conference on Computer Vision and Pattern Recognition*, 2023, pp. 19 358–19 369.
- [70] Y. Zhan, Y. Zhu, H. Zhao, F. Yang, M. Tang, and J. Wang, “Griffon v2: Advancing multi-modal perception with high-resolution scaling and visual-language co-referring,” in *Proceedings of European Conference on Computer Vision*, 2024.